Chapter 4

Spherulitic growth of hen egg-white lysozyme crystals

In protein crystallography spherulites are considered the result of a failed crystallisation experiment. Understanding the formation of these structures may contribute to finding methods to prevent their formation. Here we present an in-situ study on lysozyme spherulites grown from sodium nitrate and sodium thiocyanate solutions, investigating their morphology and growth kinetics using optical microscopy. In a morphodrom we indicate the conditions at which spherulites form for the lysozyme-nitrate system, showing that liquid-liquid phase separation is not a prerequisite to form sheave-like spherulites and that supersaturation is not the only factor determining their creation. Despite their sheave-like morphology the spherulites all appear to be formed through heterogeneous nucleation. The spherulites are of a new polymorphic form and are less stable than the monoclinic form. For a single needle growth kinetics indicate surface processes to be the rate limiting step during growth, but for an entire spherulite volume diffusion still plays a role. Spherulites simulated by using a time dependent tip splitting model are found to compare well to experimentally observed spherulites.

4.1   Introduction

X-ray diffraction (XRD) is the main route towards structure determination
of protein macromolecules. The success of a structure determination by this
method depends on the quality of the crystal. Trial-and-error methods are of-
ten used to find the proper crystallisation conditions for a specific protein. In
this process of screening of protein crystallisation conditions most experiments
do not yield XRD quality single crystals. Often the system does not exhibit
crystal nucleation at all, or precipitates amorphously [1], depending on the
degree of supersaturation of the system. In addition, proteins frequently pre-
cipitate in the form of spherulites [2, 3], also known as a "sea urchin" crystal
morphology[4]. Spherulitic growth is a generic term for the formation of radial
arrays of crystalline needles [5]. Although the term "spherulite" suggests an
approximately spherical form, it is used in a broader sense for various forms of
densely branched, polycrystalline solidification patterns [6] originating from a
common initial nucleation point. It is also used as a term for radial patterns of
fibres, for instance fibres formed by the gelling of the protein deoxyhemoglobin
S [7]. In polymer science[5, 8], biomineralisation[9, 10] and mineralogy[11]
spherulitic growth is an extensively studied phenomenon. For crystallisation
from the melt, Keith and Padden[12] indicated the presence of static hetero-
geneities (e.g. impurities or polydispersity) to cause the non-crystallographic
branching typical for the spherulitic growth form. On the other hand, spher-
ulites found in pure liquids[13] indicate that the presence of impurities cannot
be a general explanation of the spherulitic growth form. In the closely related
phenomenon of the formation of nanocrystalline fibre networks, which may
lead to the formation of spherulites[14, 15], the branching structure is formed
by crystallographic mismatch branching[16–18]. This process has been studied
in detail and is shown to be controlled by adding additives[16] or by changing
supersaturation[17]. In protein crystal growth, spherulites are often observed
(e.g. [19, 20]) but little attention has been offered to the mechanisms forming
them.

In general, protein spherulites are discarded as a failure, since they do
not yield usable XRD patterns. Understanding protein spherulite growth may

contribute to finding methods to prevent their formation. Hen egg-white lyso-zyme (HEWL) is often used as a model compound for understanding protein crystal growth in general, usually focusing on its tetragonal form obtained from sodium chloride solutions. Spherulitic growth of HEWL has been observed in liquid-liquid phase-separated lysozyme-chloride systems, and thus the formation of spherulites is thought to be a consequence of the presence of high-density phase droplets[3, 4]. Literature data indicate that spherulitic growth in these systems is controlled by surface kinetics[21].

In this paper we focus on spherulitic growth of HEWL in sodium nitrate and thiocyanate solutions, investigating in detail the morphology of individual spherulites. The objective is to improve the understanding of the formation and growth of protein spherulites.

4.2   Experimental procedures

Chemicals of analytical grade were used in this study. A buffer stock solution of sodium acetate and acetic acid was made in deionised water (>15 MΩcm) to result in a 0.05 M NaCH$_3$COO/HCH$_3$COO solution of pH 4.5. HEWL from Sigma-Aldrich (lot nr. 094K1454) was used as source material for crystal growth after purification by dialysis (MWCO 8 kDa) in buffer solution. NaNO$_3$ and NaSCN stock solutions were also prepared in buffer solution. Lysozyme, salt and buffer solutions were filtered over a 0.2 μm membrane (Schleicher & Schuell), and mixed with each other in the appropriate proportions just prior to the growth experiments.

A 1 μl droplet of the resulting mother liquor is placed between two microscope cover-slides, forming an approximately 10 μm thick layer, and is sealed off along the sides by immersion oil to prevent evaporation. Spherulites growing between two cover slides result in 2D objects, which are more suitable for imaging than 3D spherulites. The cover slides are placed, either in a temperature-controlled box for multiple, simultaneous experiments, or in a temperature controlled cell for in-situ optical microscopy. Experiments were performed at 18 ^{o}C with an accuracy of 0.1 ^{o}C and 0.5 ^{o}C respectively. The in-

situ cell consists of a brass plate through which water from a thermostatically controlled reservoir can flow. The cover slides are placed on top of the brass plate and are covered by another brass plate without water flow throughput. A 6 mm hole and a 15 mm hole at the centre of the bottom and top brass plate respectively allow for optical transmission microscopy.

Observations of the spherulites were made mainly by optical microscopy. Attempts to observe the crystal patterns by atomic force microscopy and cryo-scanning electron microscopy were not successful. A Zeiss Axioplan 2 microscope and an Olympus Vanox microscope were used, both suitable for polarisation microscopy. Higher magnification images were made using an Olympus oil immersion objective of 1.30 numerical aperture. To investigate the growth kinetics of the spherulites, series of images were recorded by time lapse CCD-photography. To determine the growth speed, the size of the spherulites in subsequent images was measured with the help of image processing software (Image-Pro Plus).

4.3 Results and discussions

4.3.1 Morphodrom

The typical morphology of 2D spherulites grown in $NaNO_3$ and NaSCN solutions is shown in figure 4.1. The conditions at which this type of structures form were investigated for the $NaNO_3$ system at 18 ^{o}C. The $NaNO_3$ concentration was varied between 0.2 M and 1 M, while the HEWL concentration ranged from 5 mg/ml up to 30 mg/ml. The presence or absence of spherulites and monoclinic crystals was verified by optical microscopy after growth in the temperature controlled box during several hours, typically needed for spherulites to form and reach their maximum size. Figure 4.2 shows the resulting morphodrom for this system, including the conditions at which liquid-liquid phase separation was observed. The solid line indicates the solubility of the monoclinic crystals as reported in literature[22]. Triclinic crystals, the stable
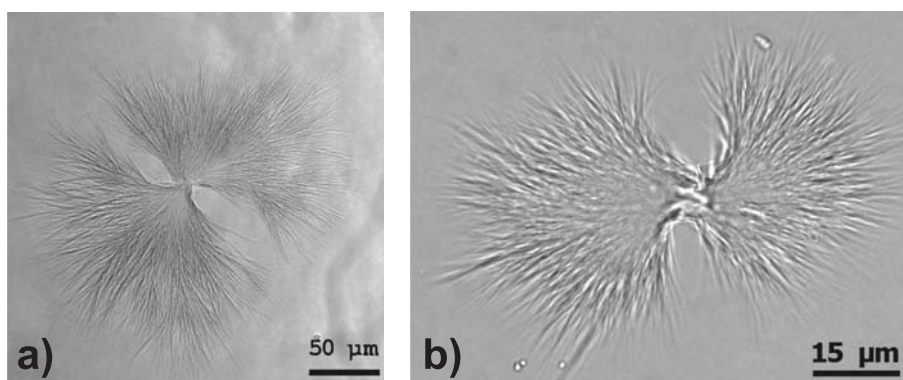
Figure 4.1: The morphology of two-dimensional HEWL spherulites grown at 18 ^{o}C in a 0.05 M sodium acetate buffer solution of pH 4.5 with a) 1 M NaNO$_3$, and b) 0.2 M NaSCN as crystallising agent, and 29 mg/ml HEWL.

polymorph* in this system and optically distinct from the monoclinic form by its crystal habit[23], were not found for these conditions.

Spherulites frequently coexist with monoclinic crystals, which in most cases appear before the spherulites do. When the temperature was raised to 28 ^{o}C, the spherulites dissolved, while the monoclinic crystals continued to grow (figure 4.3). Because the monoclinic crystals are metastable with respect to the triclinic polymorphs, the spherulites are thus a third, metastable, polymorph in the lysozyme-nitrate system. This observation does not follow Oswald's Rule of Stages, which postulates that the most metastable polymorph is the one to appear first[24]. Although powder diffraction on thick lysozyme needles is possible according to Ref. [25], in our case the needles were too thin for this method and the crystal structure of our spherulites remains unknown. From the morphodrom it follows that in order to avoid the formation of spherulites, it is better to choose a low NaNO$_3$ concentration and a high HEWL concentration than vice versa, although both mixtures can be chosen to be equally

---

*In principle, the various possible phases of the lysozyme in the nitrate system are not polymorphs in the strictest sense of the word, because their water and salt composition will vary somewhat.
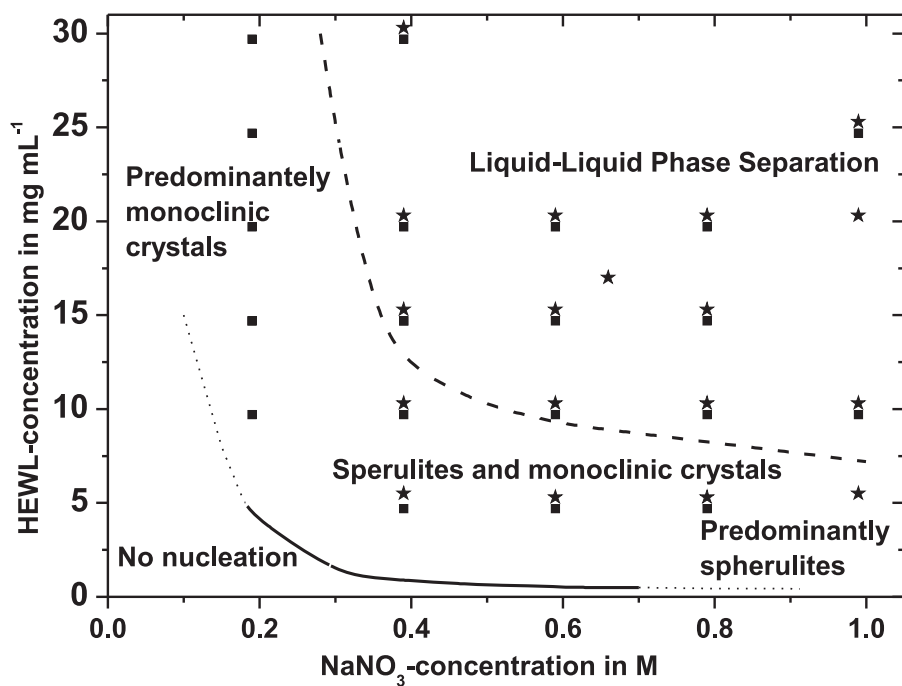
Figure 4.2: The morphodrom of the HEWL/NaNO$_3$/NaCH$_3$COO system at 18$\pm$0.5 ^{o}C and pH 4.5. Stars indicate the presence of spherulites, squares indicate the presence of monoclinic crystals. All experiments above the dashed line exhibit liquid-liquid phase separation. The solid line indicates the solubility of monoclinic HEWL, taken from literature [22], which is extrapolated to lower and higher NaNO$_3$ concentrations (dotted line) by assuming a normal solubility behaviour.
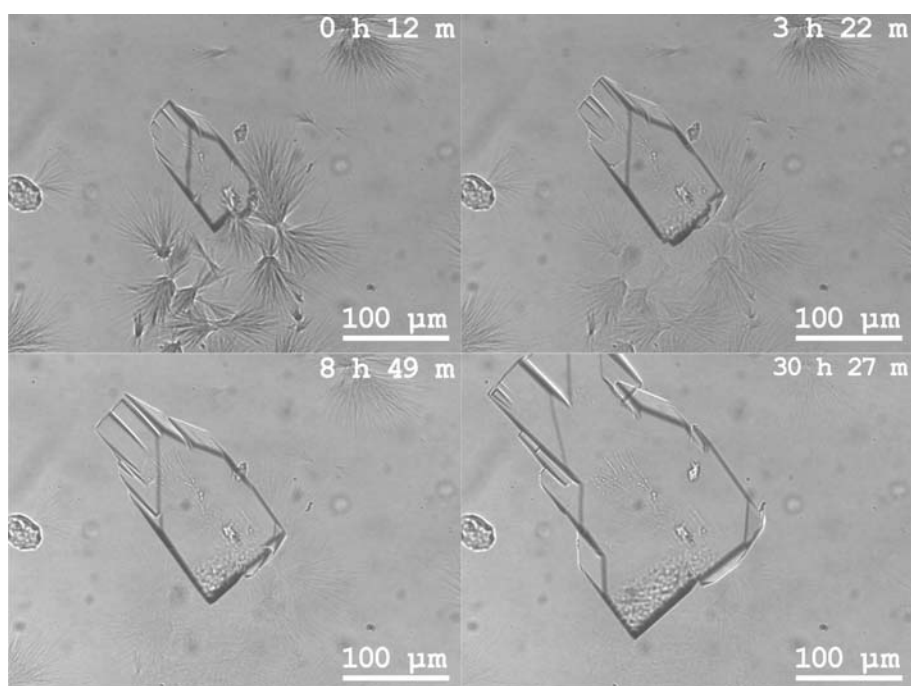
Figure 4.3: Series of in-situ optical micrographs of HEWL spherulites and a monoclinic HEWL crystal coexisting in the same solution, grown at 18^oC from a 15 mg/ml HEWL, 0.6 M $NaNO_3$ and 0.05 M $NaCH_3COO/HCH_3COO$ buffer solution at pH 4.5. Due to a raise in temperature up to 30^oC, the spherulites dissolve while at the same time the monoclinic crystal continues to grow. Time since the temperature raise is indicated in the upper right corner of the micrographs.

supersaturated with respect to the monoclinic polymorph. Thus, increasing solute concentration appears to be a better strategy to prevent spherulite formation than modifying the solvent properties by increasing the salt concentration, which changes the ionic strength of the solution.

The spherulites grown in sodium thiocyanate solutions show similar behaviour with respect to their stable monoclinic counterpart. This implies that also in the lysozyme-thiocyanate system the spherulites form a second, metastable, polymorph.

In literature, the nucleation of protein spherulites is often associated with the presence of liquid-liquid phase separation[3, 4, 21, 25]. The small gelled protein droplets might act as heterogeneous nuclei for the needles. However, we found that the number of spherulites found in phase separated systems did not differ greatly from the number of spherulites in non-separated systems. The nucleation probably occurs heterogeneously, because more spherulites were observed in the presence of foreign particles, i.e. when using stock solution without filtering.

4.3.2   Morphology of spherulites

Spherulites are often divided into two morphologic categories, which differ in the nucleation mechanism[5]. Type I is assumed to be a result of heterogeneous nucleation, with thin needles radially growing outward from a more or less spherical particle (figure 4.4a). The second type is thought to be the result of homogeneous nucleation. A single needle is formed by homogeneous nucleation, which subsequently branches leading to a *sheave*-like morphology (figure 4.4b). After continued growth, the branching can even result in both ends of the dumbbell shaped spherulite touching, creating a spherical shape with cavities inside.

Clearly, the spherulites in our experiment resemble type-II spherulites, with similar morphologies independent of salt and lysozyme concentration. In growth cells with large spacing in the third dimension the sheave-like spherulites can also resemble type-I spherulites, when viewed along their longitudinal axis (figure 4.5). However, in the experiments with a maximum of 10 μm of
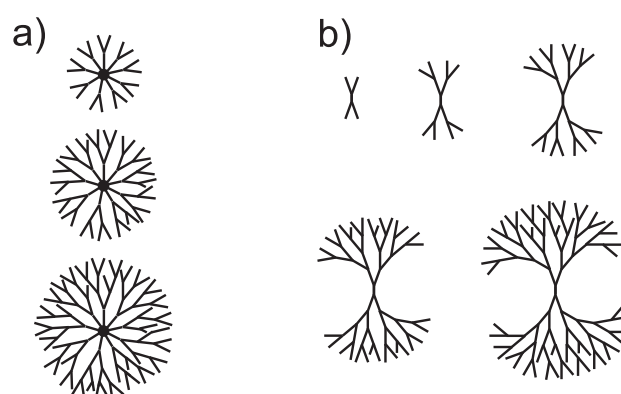
Figure 4.4: Schematic representation of the formation of spherulites. a) Type 1 spherulites are formed by heterogeneous nucleation on a foreign particle, for instance a dust particle. Crystalline needles radiate outward from this nucleus. b) Type 2 spherulites form by the homogeneous nucleation of a single crystalline needle, which subsequently grows and branches off.
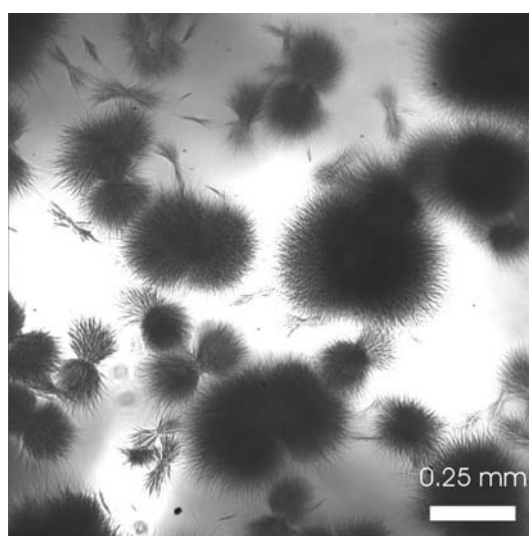
Figure 4.5: Spherulites grown from a 40 mg/ml HEWL / 0.2 M NaNO$_3$ / 0.05 M NaCH$_3$COO solution in a 2 ml vessel (5 mm in height), resulting in three-dimensional spherulites. Viewed from different angles, the spherulites seem to have different shapes.

space in between the cover slides, all spherulites are sheave-like. The sheave-like spherulites also form when no filtering is applied to the solution, in which case one would expect type I spherulites as well. Thus, in the case of lyso-zyme spherulites, the customary classification into the two types does not hold. The nucleation needs not to be homogeneous to form a sheave-like spherulite following the scheme of figure 4.4b. A single needle can nucleate either homo-geneously or heterogeneously, after which the type-II spherulites form. Due to filtering of the mother liquor, the foreign particle on which nucleation oc-curs is expected to be smaller than the 0.2 μm filter pores, and thus can be incorporated completely in the needle, allowing the spherulite to develop in opposite directions.

During growth, the needles of the spherulites exhibit repeated tip splitting, with an angle of 20 ± 5° in the sodium-nitrate experiments and 19 ± 7° in the sodium-thiocyanate experiments. The branching angles thus are preferential with a spread of approximately 10°, indicating a mechanism for tip splitting similar to crystallographic mismatch branching (CMB)[16, 17]. In CMB, het-erogeneous 3D nucleation, for instance induced by additives adsorbed to the needle tip cause the needle to split in preferred directions, with the needle tip acting as a template. An experiment using ultra-pure lysozyme (99.99%, Mol Logics Inc, Japan) was performed in which spherulites with identical properties did form, indicating that foreign additives are not involved. Presumably the "additives" triggering tip splitting are either misoriented lysozyme molecules or clusters of molecules. The measured spread in the branching angle is in-creased by uncertainties induced by the fact that the needles often have some curvature (figure 4.1a).

From the optical images we find that the thickness of the needles depends on the distance from the spherulite centre, with the thick needles located at the centre and the thin needles near the periphery. The width of the outer needles is at most 1 μm, which is explained by the fact that these crystallites have had less time to grow. Also, the branching frequency depends on the distance from the growth centre, leading to longer branches on the outside.

When the system approaches equilibrium at the end of the experiment,
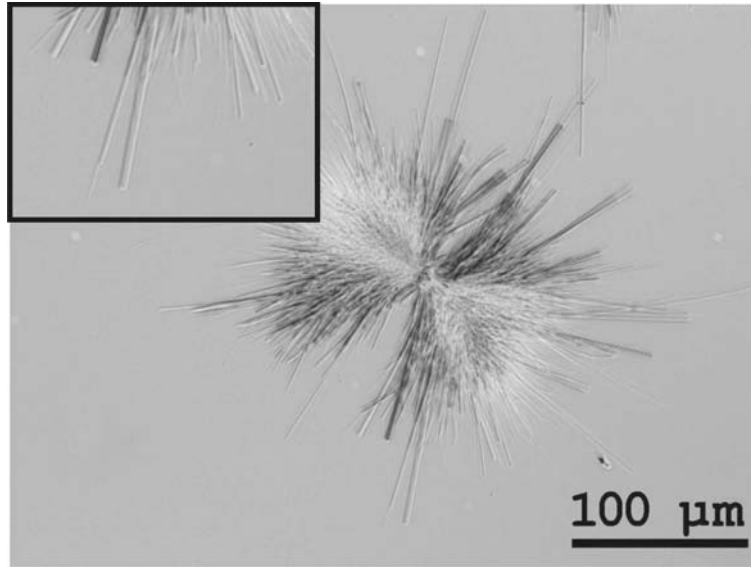
Figure 4.6: Negative of a polarisation microscope image of a spherulite with thick needles sticking out. As $\Delta\mu$ approaches zero, growth of the spherulites ceases. Some needles continue to grow very slowly, by which the aspect ratio also changes, as the top faces slow down with respect to the side faces and become faceted (inset). The extinction angle for the polarised light varies with the direction of the needles.

most needles cease to grow. Some of the needles continue to grow very slowly in width, depending on the local HEWL concentration. The width of these needles increases up to ~ 5 μm. The aspect ratio of the needles decreases and the tips of the needles become faceted (figure 4.6). These faceted top faces are not present during growth, which indicates that during growth the tips are kinetically rough[26]. The needle shape is the basic morphology of the spherulitic polymorph, both at low and high supersaturation.

4.3.3   Growth kinetics and diffusion

Using the in-situ temperature-controlled cell, the growth kinetics of the spherulites were investigated. In various experiments, the growth rate of spheru-

lites was determined from a time series of microscope CCD-images. Figure
4.7 shows a series of in-situ images of a spherulite growing from a buffered
$NaNO_3$ solution. The growth rates of the spherulites were determined by av-
eraging over an angular section of the spherulites as indicated in figure 4.7.
The spherulite size is calculated by dividing the surface area of the angular
section by the angle β. The length of the left and right side of this spherulite
is represented as function of time in figure 4.8a. Both sides show an almost
identical, constant growth speed up to a certain point at which it drops dra-
matically, due to the growth solution being exhausted. The growth speeds
in the linear regime are 0.95±0.03 μm/min and 0.86±0.01 μm/min for the
right and left side respectively. Constant growth rates were found in all ex-
periments, also for the experiments using NaSCN as crystallising agent. This
is in agreement with observations by Chow et al.[21] for HEWL spherulites
growing from sodium chloride solutions.

In the experiments of Chow et al.[21] surface kinetics are the rate limit-
ing step for the growth process. In our experiments, however, volume dif-
fusion seems also to play an important role, because during the growth of
the spherulite the region of separated liquid-liquid phase retracts from the
spherulitic growth front (figure 4.7). This retraction is a result of spherulite
growth depleting the surrounding solution. As the concentration drops, the
high-concentration droplets dissolve to replenish the lysozyme which is needed
to maintain equilibrium at the droplet interface. Thus, the boundary of the
phase separated region can be seen as an iso-concentration line correspond-
ing with the L-L phase separation equilibrium concentration. The retracting
iso-concentration line indicates that the surroundings of the spherulite are pro-
gressively depleted, suggesting that mass transport is also relevant. However,
when we regard a single needle of the spherulite as if it were a dendrite tip[27]
with a local diffusion field around it, we can write the following expression
for the concentration difference between the bulk of the solution and at the
surface (see appendix and figure 4.9):

$$c_b - c_s = \frac{v_{\mathrm{needle}}\, R}{4\, k\, D\, V_{\mathrm{mol}}} \; , \qquad\qquad (4.1)$$
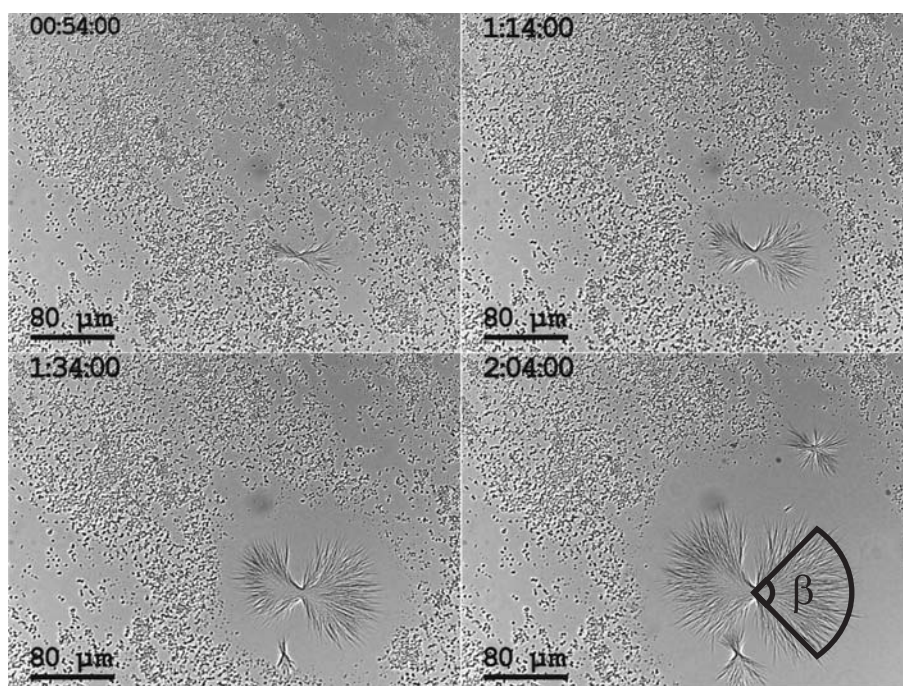
Figure 4.7: Series of images of spherulites growing in a 22 mg/ml HEWL / 0.8 M NaNO$_3$ / 0.05 M NaCH$_3$COO/HCH$_3$COO solution at 18°C and pH 4.5. Time indicated in the pictures is the time since the start of the experiment in hours-minutes-seconds. The small dots surrounding the spherulite are the liquid-liquid phase separation droplets.
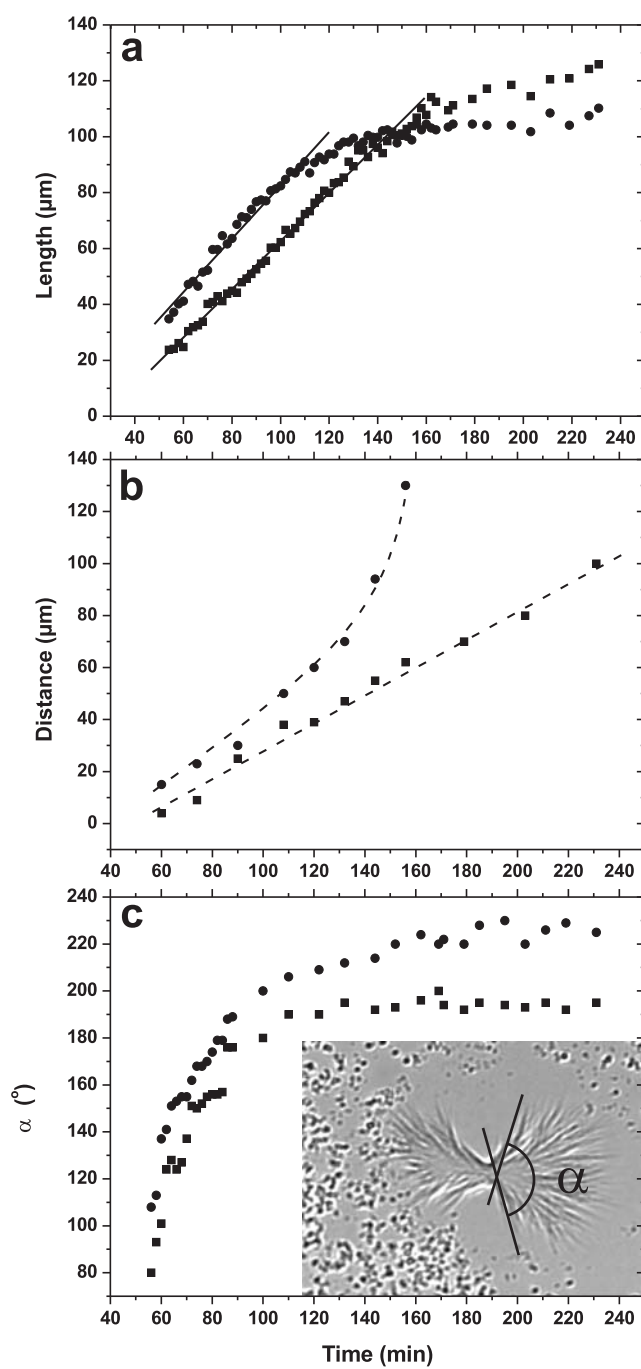
Figure 4.8: See page 74. Growth rate of the large spherulite in figure 4.7. (a)The squares indicate the length of the left side of the spherulite, and the circles indicate the length of the right side. The solid lines indicate linear fits for the surface kinetics regime. The left side has a growth rate of 0.86±0.01 μm/min, the right side 0.95±0.03 μm/min. (b) The squares and circles indicate the distance between the high-concentration droplets and the spherulite periphery for the left and right side respectively. Dashed lines are a guide to the eye. (c) The angle, α (see inset), for both the left (squares) and right (circles) side versus time.
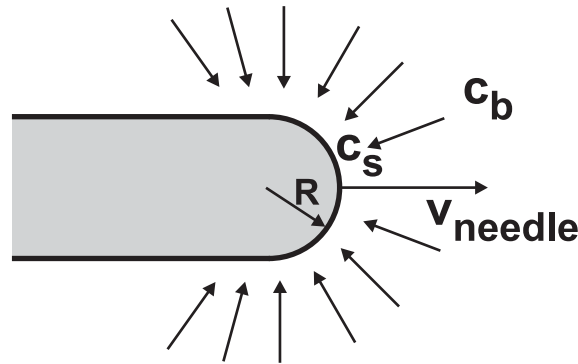
Figure 4.9: Model of a growing needle and its supply of material from its surroundings.

with c_b the bulk concentration, c_s the surface concentration, v_{needle} the growth rate of the needle, k a geometric correction factor, D the diffusion constant of lysozyme, and V_{mol} the volume of one lysozyme molecule. Taking $D = 1.2 \times 10^{-10}$ m^2/s from literature [28], and $v_{\text{needle}} = 15$ nm/s, and the needle tip radius $R = 0.5$ μm from experiment, we find a concentration difference in the order of 25 μg/ml, whereas the bulk concentration is typically in the order of 10 mg/ml, i.e. about 400 times larger. Thus, the surface concentration at the needle tips hardly drops, indicating surface kinetics to play a major role in the growth process and mass transport to have little effect.

Although for a single needle volume diffusion does not play a role, all

needles together, i.e. the spherulite as a whole, do deplete the surrounding solution. An analysis similar to the single needle analysis can be performed, resulting in (see appendix)

$$c_b - c_s = \frac{\xi \, v_{\mathrm{needle}} \, R}{D \, V_{\mathrm{mol}} \, N_A} \ln \frac{\delta}{R} \ , \qquad (4.2)$$

in which δ is the distance from the origin of the spherulite to the liquid-liquid phase separated region, R in this case the spherulite radius, and ξ a density correction factor for the fact that the spherulite is not a 100% dense structure, but has solution-filled spaces in between the needles. In a rough approximation using values for R and δ from experiment (squares in figure 4.8b) and estimating $\xi \approx 0.2$ from experiment, the spherulite surface concentration drops at a rate of 0.05 mg ml^{-1} min^{-1}. The surface concentration thus becomes significantly lower than the bulk concentration during growth, indicating that mass transport, although not the major limiting factor, plays an important role in the growth process.

The decrease in supersaturation during continued spherulite growth influences both the branching frequency of the needles and the length of the needles up to the next splitting. To determine the number of times the needles have split, we measure the angle, α, between the outermost needles (see insert in figure 4.8c) and divide it by the angle of 20° by which the needles typically split. The angle α increases with time, but stops increasing even before the needles slow down (figure 4.8c). When we plot the length of the spherulite versus the angle α, or the number of times the needles have branched, n, we find a stepwise linear dependence (figure 4.10), which indicates that the influence of decreasing supersaturation on the angle and on the length are different. Since the top faces of the needles are kinetically roughened[26], the growth rate of the needles is proportional to the supersaturation:

$$v_{\mathrm{needle}} \propto \Delta\mu \ . \qquad (4.3)$$

On the other hand, the formation of a new needle branch is a heterogeneous 3D nucleation process, which, in its simplest form, is governed by an exponential

dependency of the nucleation rate J on the driving force[16, 29]:

$$J \propto e^{-f\gamma^3/\Delta\mu^2 kT} \; , \tag{4.4}$$

with γ the edge free energy, k Boltzmann's constant and T the temperature. Further, $f = \frac{16}{3}\frac{K}{}\pi\Omega^2$ in which Ω is the volume of a growth unit and K is a constant depending on the equilibrium shape of the heterogeneous nucleus[30]. As needle growth is largely controlled by surface kinetics, a considerable supersaturation still exists at the needle tips, which makes heterogeneous nucleation quite feasible. From this it follows that any change in driving force ($\Delta\mu$) has a higher impact on the tip splitting rate than on the growth rate and the average branching length v_{needle}/J increases for decreasing $\Delta\mu$. The same conclusion was drawn by Liu et al. for the growth of branched L-DHL fibres by the CMB process[16]. Figure 4.10 shows a linear regime for the left side up to $\alpha \approx 170^o$. In this regime the branching frequency is constant, implying a constant driving force, $\frac{\Delta\mu}{kT}$ and thus surface kinetics is the rate limiting step. During further growth branching becomes limited due to depletion of the solution and by volume diffusion, which is evident from the retracting L-L phase separation droplets. For the right side, the branching frequency is constant up to an abrupt stop. Neighbouring spherulites speed up the depletion of the solution resulting in this abrupt cessation of both branching and growth. Thus, volume diffusion has a significant influence on the morphology depending on the history and surroundings of the spherulite.

4.3.4 Simulated morphologies

To investigate qualitatively the balance between needle growth and tip splitting, we developed a model to calculate the shape of a spherulite using MATLAB[31]. In this model, the spherulite starts as a single needle that splits into two new needles at each end. These new needles in their turn split up at their tip, with the angle of bifurcation and its spread taken from experiment (20 ± 5°). Repeating the process of bifurcation of the needles results in a Cayley-like tree structure[32] of which the shape depends on the relation between needle length and the number of times the needles have split. In the
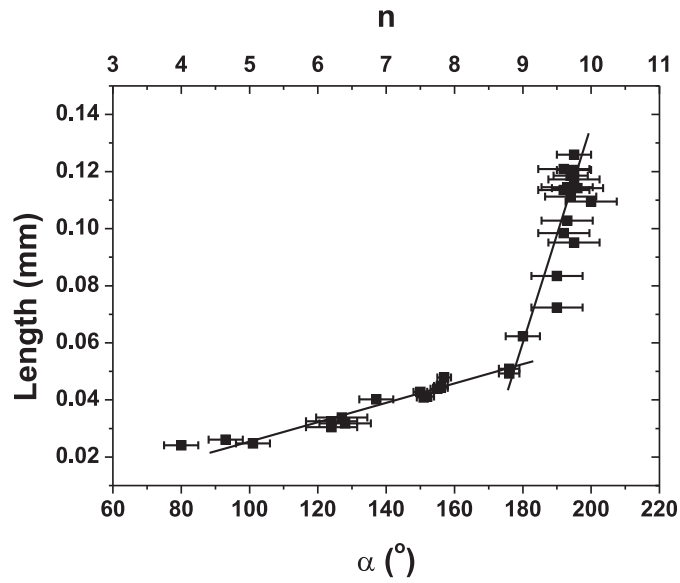
Figure 4.10: The angle, α, of the left side of the spherulite versus the length of the left side. The lines are linear fits used for the simulated morphology. n indicates the number of tip splittings.
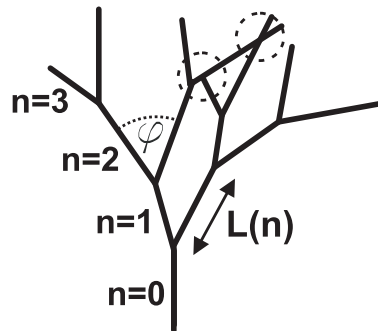
Figure 4.11: Illustration of a Cayley-like tree, showing the definition of bifurcation number n, needle length $L(n)$ and bifurcation angle φ. The length of an individual needle $L(n)$ depends on bifurcation number with an added stochastic deviation. The dashed circles indicate a needle being blocked by (left) and crossing over another needle (right).

experiments we find that needles cross over each other, but can be blocked as well. To mimic this behaviour, a blocking probability which equals the percentage of needles not surviving an encounter with another needle is added to the model (figure 4.11). The model thus builds up a Cayley-like tree with for every individual branch within a shell a stochastically different length and branching angle, and the possibility of a branch to end instead of to split.

Figures 4.12a to c show the calculated spherulite morphologies with 0%, 50% and 100% blocking probability using the two linear fits to the experimental data as indicated by the lines in figure 4.10. One fit concerns the linear surface kinetics limited regime, the second to approximate the volume diffusion limited regime, i.e.:

$$L(n) = \begin{cases} (-1.2 + 5.7n) \pm 20\% \ \mu\text{m} & n \leq 8 \\ (-512 + 65n) \pm 20\% \ \mu\text{m} & n > 8 \end{cases} \tag{4.5}$$

$L(n)$ is the needle length after the spherulite has bifurcated n times. On the basis of experimental data, the model returns a very similar morphology, indicating that tip-splitting is a viable mechanism in spherulite formation. A blocking probability of 50% results in a morphology which is most similar to experiment.

Preferably one would try equations 4.3 and 4.4 for the link between length and branching frequency in the model. However, as the nucleation rate depends on an exponential, the results strongly depend on the exponential and pre-exponential factor, which are difficult to determine from experiment. However, to illustrate the influence of the branching kinetics on the morphology, we used a few simple relations for $L(n)$. Figure 4.12d up to f show several model spherulites with a 50% blocking probability, with needle length $L(n)$ =constant, $L(n) = n$ and $L(n) = n^2$ respectively. The morphology clearly varies with the chosen relation between needle length and bifurcation number, especially the shape of the "eyes" of the spherulite. A constant branch length results in a very large, circular eye, while dependencies with excessively increasing needle-length produce long and narrow eyes. The relation $L(n) = n^2$ resembles the experiment most closely.
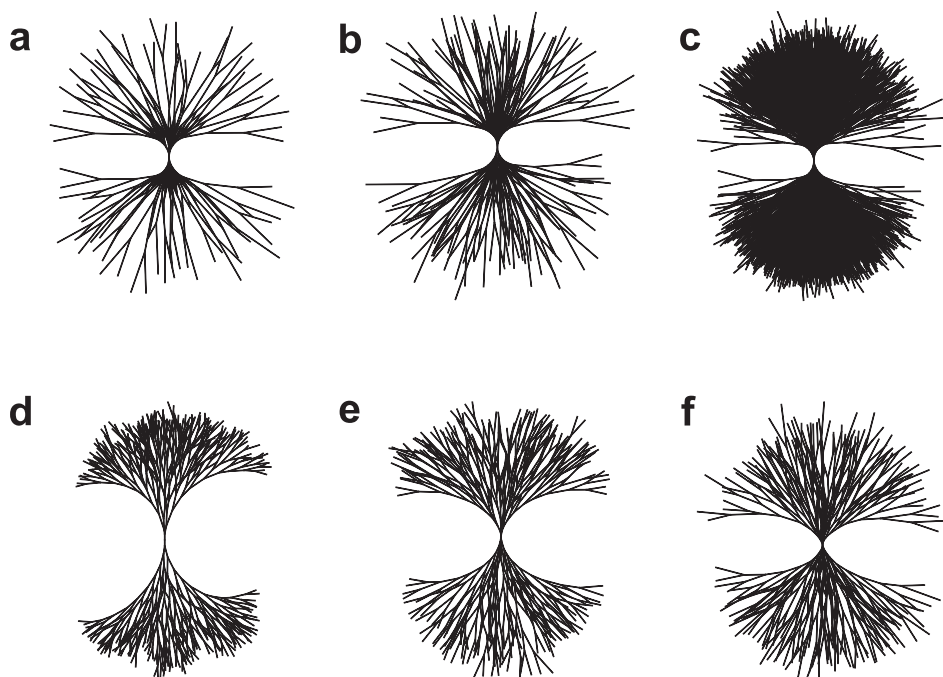
Figure 4.12: Calculated morphologies of spherulites based on the tip splitting mechanism. Panels a till c are calculations using linear fits to experiment, and a blocking probability of a) 100%, b) 50% and c) 0%. Panels d till f show calculated morphologies at a blocking probability of 50% for d) $L(n)$, the length of a branch as function of the number of tip splittings that have occurred, is constant, e) $L(n) = n$, and f) $L(n) = n^2$.

4.4 Conclusions

Hen egg-white lysozyme spherulites can be grown from NaNO$_3$ and NaSCN solutions. In both systems the needle-like crystals composing the spherulites are metastable with respect to the known HEWL protein phases. We conclude that HEWL spherulites grown from both solutions mainly grow in a sheave-like morphology, with very fine needles branching within a range of preferred angles suggesting crystallographic mismatch branching[16, 17]. Growth kinetics for the nitrate system indicate that surface kinetics largely limits the growth rate of an individual needle, while on the other hand the expanding depletion of the liquid-liquid phase separation region shows that volume diffusion can not be neglected for the spherulite as a whole. Observed and simulated morphologies indicate that volume diffusion limitation significantly influences the branching morphology of the spherulites. In general, choosing a high lysozyme concentration and a low NaNO$_3$ concentration prevents spherulite formation.

Acknowledgements

Appendix A: Stationary approximation of the diffusion fields around single needles, and around the complete spherulite

The spherulite needle can be regarded as a dendrite tip with a local diffusion field around it[27]. As the needle grows slowly compared to typical dendritic growth, the stationary approximation can be assumed. Thus, the surface of the needle does not move, and the concentration profile is time-independent. For a single needle, the system can be considered 3D as the needle thickness of $\approx 1~\mu$m is much less than the liquid layer in the growth cell of $10~\mu$m. Thus, mass transport for the local surroundings of the needle tip can be described

by solving Fick's equations $\nabla^2 c=0$ and $\vec{J} = -D\vec{\nabla}c$ in spherical coordinates, i.e.

$$\frac{\mathrm{d}^2 c}{\mathrm{d}r^2} + \frac{2}{r}\frac{\mathrm{d}c}{\mathrm{d}r} = 0 \ . \tag{A.1}$$

Using boundary conditions at the needle tip and at large distance away (i.e. at infinity) the standard solution for equation A.1 becomes

$$c(r) = \frac{R\,(c_s - c_b)}{r} + c_b \ , \tag{A.2}$$

in which R is the radius of the needle tip (see figure 4.9), c_s the concentration at the surface, and c_b the bulk concentration. Using Fick's first law in spherical coordinates, $J = -D\frac{\mathrm{d}}{\mathrm{d}r}c$, we find the flux J of mass *into* the needle tip

$$J(R) = D\,\frac{c_b - c_s}{R} \ , \tag{A.3}$$

in which D is the diffusion constant of lysozyme. The gain in volume of the needle per unit time $\frac{\mathrm{d}V}{\mathrm{d}t}$ is related to this flux by

$$\begin{aligned}
\frac{\mathrm{d}V}{\mathrm{d}t} &= 4\pi\,R^2\,k\,V_{\mathrm{mol}}\,N_A\,J \\
&= 4\pi\,R\,k\,V_{\mathrm{mol}}\,N_A\,D\,(c_b - c_s) \ ,
\end{aligned} \tag{A.4}$$

in which $\frac{1}{2} \leq k \leq 1$ is a factor to compensate for the fact that the top of the needle is not a complete sphere (figure 4.9), V_{mol} the volume of one HEWL molecule, and N_A Avogadro's number. The volume increase can also be expressed in terms of the growth speed of the needle, v_{needle}:

$$\frac{\mathrm{d}V}{\mathrm{d}t} = \pi\,R^2\,v_{\mathrm{needle}} \ . \tag{A.5}$$

Thus, substituting equation A.5 in A.4 results in an expression for the difference between surface concentration and bulk concentration:

$$c_b - c_s = \frac{v_{\mathrm{needle}}\,R}{4\,k\,D\,V_{\mathrm{mol}}\,N_A} \ . \tag{A.6}$$

The spherulite as a whole can be approximated by a flat cylinder and thus the cylindrical instead of the spherical form of Fick's laws has to be used:

$$\frac{\mathrm{d}^2 c}{\mathrm{d}r^2} + \frac{1}{r}\frac{\mathrm{d}c}{\mathrm{d}r} = 0 \ , \tag{A.7}$$

with the general solution

$$c(r) = a \ln r + b \, . \tag{A.8}$$

In this case we cannot take the boundary condition at $r = \infty$, but we have to choose a finite distance δ for c_b. A logical choice is the perimeter of the liquid-liquid phase separated region. Although experiment clearly shows that the concentration profile cannot be considered stationary, it is a good and often used first approximation to consider the system stationary for any point in time. The concentration profile at such a time is a function of r and is given by

$$c(r) = c_s + \frac{c_s - c_b}{\ln \frac{R}{\delta}} \ln \frac{r}{R} \, . \tag{A.9}$$

Following the same route as for the single needle case we find an expression for the concentration difference $c_b - c_s$

$$c_b - c_s = \frac{\xi \, v_{\text{needle}} \, R}{D \, V_{\text{mol}} \, N_A} \ln \frac{\delta}{R} \, , \tag{A.10}$$

in which ξ is a density correction factor for the fact that the spherulite is not a 100% dense structure but has solution-filled spaces in between the needles. The rate by which the surface concentration drops can be determined by substituting values for R and δ taken from subsequent images into equation A.10.

References

[1] McPherson, A. *Crystallization of Biological Macromolecules;* Cold Spring Harbor Laboratory Press: New York, 1999.

[2] Coleman, J.; Allan, B.; Vallee, B. *Science* **1960,** *131,* 350-352.

[3] Tanaka, S.; Yamamoto, M.; Ito, K.; Hayakawa, R.; Ataka, M. *Phys. Rev. E* **1997,** *56,* R67.

[4] Muschol, M.; Rosenberger, F. *J. Chem. Phys.* **1997,** *107,* 1953-1962.

[5] Philips, P. . In *Handbook of Crystal growth*, Vol. 2; Elsevier: Amsterdam, 1993; Chapter 18, pages 1169–1216.

[6] Gránásy, L.; Pusztai, T.; Tegze, G.; Warren, J.; Douglas, J. *Phys. Rev. E* **2005,** *72,* Art. No. 011605.

[7] Briehl, R. *J. Mol. Biol.* **1995,** *245,* 710-723.

[8] Magill, J. *J. Mater. Sci.* **2001,** *36,* 3143-3164.

[9] Prymak, O.; Sokolova, V.; Peitsch, T.; Epple, M. *Cryst. Growth Des.* **2006,** *6,* 498-506.

[10] Grases, F.; Villacampa, A.; Costa-Bauza, A. *Urological Research* **1999,** *27,* 141-147.

[11] Wang, Q.; Morse, J. *Mar. Chem.* **1996,** *52,* 99-121.

[12] Keith, H. D.; Padden, F. J. *J. Appl. Phys.* **1963,** *34,* 2409-2421.

[13] Bisault, J.; Ryschenkow, G.; Faivre, G. *J. Cryst. Growth* **1991,** *110,* 889-909.

[14] Liu, X. *Top. Curr. Chem.* **2005,** *256,* 1-37.

[15] Wang, R.; Liu, X.; Xiong, J.; Li, J. *J. Phys. Chem. B* **2006,** *110,* 7275-7280.

[16] Liu, X. Y.; Sawant, P. D.; Tan, W. B.; Noor, I. B. M.; Pramesti, C.; Chen, B. H. *J. Am. Chem. Soc.* **2002,** *124,* 15055-15063.

[17] Li, J. L.; Liu, X. Y.; Wang, R. Y.; Xiong, J. X. *J. Phys. Chem. B* **2005,** *109,* 24231-24235.

[18] Liu, X. Y.; Sawant, P. D. *Adv. Mater.* **2002,** *14,* 421-426.

[19] Echalier, A.; Glazer, R.; Fülöp, V.; Geday, M. *Biol. Crys.* **2004,** *60,* 696-702.

[20] Guilloteau, J.; Fromage, N.; Ries-Kautt, M.; Reboul, S.; Bocquet, D.; Dubois, H.; Faucher, D.; Colonna, C.; Ducruix, A.; Becquart, J. *Proteins* **1996,** *25*, 112-119.

[21] Chow, P.; Liu, X.; Zhang, J.; Tan, R. *Appl. Phys. Lett.* **2002,** *81*, 1975-1977.

[22] Guilloteau, J.; Riès-Kautt, M.; Ducruix, A. *J. Cryst. Growth* **1992,** *122*, 223-230.

[23] Heijna, M.; van den Dungen, P.; van Enckevort, W.; Vlieg, E. *Cryst. Growth Des.* **2006,** *6*, 1206-1213.

[24] Ostwald, W. *Z. Phys. Chem.* **1897,** *22*, 289-230.

[25] Bhamidi, V.; Skrzypczak-Jankun, E.; Schall, C. *J. Cryst. Growth* **2001,** *232*, 77-85.

[26] van Veenendaal, E.; van Hoof, P.; van Suchtelen, J.; van Enckevort, W.; Bennema, P. *Surf. Sci.* **1998,** *417*, 121-138.

[27] Glicksman, M.; Marsh, S. . In *Handbook of Crystal Growth*, Vol. 1; Elsevier: Amsterdam, 1993; Chapter 15, pages 1082–1085.

[28] Kim, Y.; Myerson, A. *J. Cryst. Growth* **1994,** *143*, 79-85.

[29] Kashchiev, D.; van Rosmalen, G. *Cryst. Res. Technol.* **2003,** *38*, 555-574.

[30] Mutaftschiev, B. . In *Handbook of Crystal growth*, Vol. 1; Elsevier: Amsterdam, 1993; Chapter 4, page 208.

[31] MATLAB 6.5 (Release 13), The MathWorks Inc.

[32] Cayley, A. *Philos. Mag.* **1858,** *28*, 374.